

Symmetry-breaking of single-particle and of many-particle electron states in self-assembled InAs/GaAs quantum dot-molecules

Lixin He, Gabriel Bester, and Alex Zunger
 National Renewable Energy Laboratory, Golden, Colorado 80401
 (Dated: January 27, 2020)

We observed two forms of wave function symmetry-breaking for two electrons in a quantum dot-molecule made of vertically stacked, strained InAs/GaAs self-assembled dots. First, the single-particle "molecular orbitals" deviate at short interdot separation $d = 3.4$ nm from the delocalized, bonding/antibonding picture, showing instead a strain-induced localization of the lowest energy orbital on the bottom dot, and of the next orbital on the top dot. Second, whereas the many-particle wave functions of the lowest singlet 1S and triplet 3S states show that the two electrons are delocalized on the two dots within the molecule, for the next singlet states 1D two electrons are localized on the same (bottom) dot for interdot separation $d > 8$ nm. The singlet-triplet splitting is found to be as large as 100 m eV for short interdot distances, much larger than the few m eV found in the large (50–100 nm) electrostatically confined dots tested previously.

PACS numbers: 73.63.Kv, 85.35.-p, 73.23.Hk

Quantum dot-molecules (QDM) occupied by two electronic spins have been proposed as a basis for quantum computation.¹ Loss and DiCarlo² proposed a "swap gate" based on a simplified model in which the two localized spins have Heisenberg coupling $H = J_{S_T} S_1 S_2$, where S_1 and S_2 are the spin- $\frac{1}{2}$ operators for the two localized electrons, and J_{S_T} is the effective Heisenberg exchange splitting, being the difference in energy between the spin-triplet state with total spin $S = 1$ and the spin-singlet with $S = 0$. Successful operation would require a large-singlet triplet splitting J_{S_T} (fast swap time²), and that the probability $Q_{\text{tot}}^{(1)}$ of the two electrons in state simultaneously occupying one dot be small (maximizing entanglement³). The search for a nanosystem with large J_{S_T} and small $Q_{\text{tot}}^{(1)}$ involves engineering of the properties of the corresponding many-particle wave functions. In a simplified molecular model, the single-particle wave functions of the two electrons are given by bonding $\psi_{\text{b}} = (\psi_T + \psi_B) = \frac{1}{2}$ and antibonding $\psi_{\text{a}} = (\psi_T - \psi_B) = \frac{1}{2}$ molecular orbitals, constructed from the individual orbitals of the top (T) and bottom (B) dot. The many-particle states are then the corresponding product states $j_g^1 i^1 g$ (singlet), and $j_g^1 i^3 g$ (triplet), etc. In this picture both single-particle molecular orbitals and the many-particle states are delocalized on both dots constituting the dot-molecule. Here we discuss via realistic single-particle and many-body calculations two important deviations from this simplified molecular picture, leading to a symmetry-breaking (i.e. localization either on T or on B) both in the single-particle molecular orbitals and in the many-body states. We show a strain-induced bottom dot localization of the lowest energy single-particle molecular orbital. For the many-body states we find Mott-like transitions for the first and third singlet states: both electrons are localized on one dot at large d and delocalized over both dots at small d . The double occupancy $Q_{\text{tot}}^{(1)}$ of the first singlet state is surprisingly large (~40%) for an interdot

separation of 5 nm. The triplet states and the second singlet state are Mott-localized at every interdot separations with $Q_{\text{tot}}^{(1)} = 0$ (no double occupation) for the triplet states and $Q_{\text{tot}}^{(1)} = 1$ for the singlet state.

Previous models of dot-molecules have focused on electrostatically-confined dots^{4,5,6}, which have a very large confining dimension of 50–100 nm. Such dots exhibit typical single-particle level spacings of $\epsilon = 3$ –5 m eV, Coulomb energies J_{ee} of about 5 m eV^{7,8}, whereas exchange energies and correlation energies are around 1 m eV. Many experiments were recently done on two such coupled dots^{7,8}, showing that the splitting between the bonding and antibonding molecular levels is as large as 3.5 m eV at an interdot separation of 2.5 nm, comparable to the single-particle energy spacing ϵ of the single dot. Because of the very large size of such dots, their single-particle levels can be described by simple one-band effective mass "particle in a box" models using the external potential generated by a combination of band offset, the gate potential and the ionized impurities.^{9,10} Alternatively, one can simply assume a particle-in-a-parabolic well model^{11,12}. In these descriptions, there is no symmetry-breaking in the single-particle states, but many-electron symmetry breaking is possible due to correlation effect, as shown via unrestricted Hartree-Fock treatment of the effective-mass approximation (UHF-EM Λ),¹³ or configuration-interaction treatment of the effective-mass approximation (CIEM Λ).¹²

Here, we discuss localization effects and singlet-triplet splitting of electrons in vertically coupled self-assembled InAs/GaAs quantum dot molecules grown epitaxially^{14,15,16}. Such dots have much smaller confining dimensions (height of 3–5 nm), and when made of InAs/GaAs their electronic level splitting is $\epsilon = 40$ –50 m eV, larger than the interelectronic Coulomb repulsion $J_{ee} = 10$ –20 m eV, and the exchange energy $K_{ee} = 2$ –5 m eV. In this paper, we show that in vertically aligned self-assembled dots, one can achieve singlet-triplet splittings of up to 100 m eV, but that this quantity reflects two

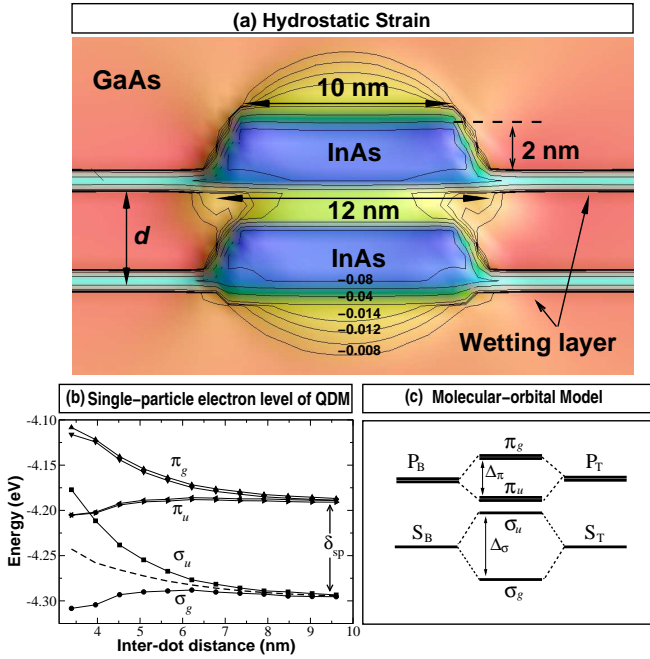


FIG. 1: (a) (Color online) Contour plot of the hydrostatic strain $\text{Tr}(\epsilon)$ in the two vertically coupled quantum dots. The inter-dot distance d is measured from one wetting layer to the next. (b) Molecular orbital energy levels vs. inter-dot distance. The dashed line is the average of σ_g and σ_u . δ_{sp} is the single dot sp energy level splitting. (c) Sketch of bonding-antibonding splitting. S_T, S_B are "s" while P_T and P_B are "p" single dot orbitals on top and bottom dots. Here $S_T + S_B = \sigma_g$ and $P_T + P_B = \sigma_u$ are bonding states, while the $S_T - S_B = \sigma_u$ and $P_T - P_B = \sigma_g$ are antibonding states.

types of wave function symmetry breaking noted above.

Figure 1a shows the geometry selected for the dot molecules, consisting of two-dimensional InAs wetting layers, a pair of 2 nm tall InAs dots in the shape of truncated cones embedded in a GaAs matrix. The hydrostatic strain field $\text{Tr}(\epsilon)$, as plotted in Fig. 1a, is calculated atomistically by relaxing the bond-stretching and bond-bending forces according to the valence force field model (VFF).^{17,18} It is clearly seen in Fig. 1a that both dots have large and nearly constant hydrostatic strain inside the dots which decays rapidly outside the dots. However, even though the dots comprising the molecule are the same, the strain on the two dots is different since the molecule lacks inversion symmetry. We see that the top dot is slightly more strained than the bottom dot. Furthermore, the GaAs region between the two dots is much more strained than in other parts of the matrix.

Having established a realistic geometry and the relaxed atomic positions \mathbf{r}_m , \mathbf{g} , we calculate the single-particle electron structure by constructing a pseudopotential $V(\mathbf{r}) = \sum_m v_m(\mathbf{r} - \mathbf{R}_m, \mathbf{g})$ from a superposition of screened atomic potentials v_m of species $m = \text{Ga, In, As}$. Here, v_m is constructed¹⁹ by fitting to available experimental data the bulk InAs and GaAs band ener-

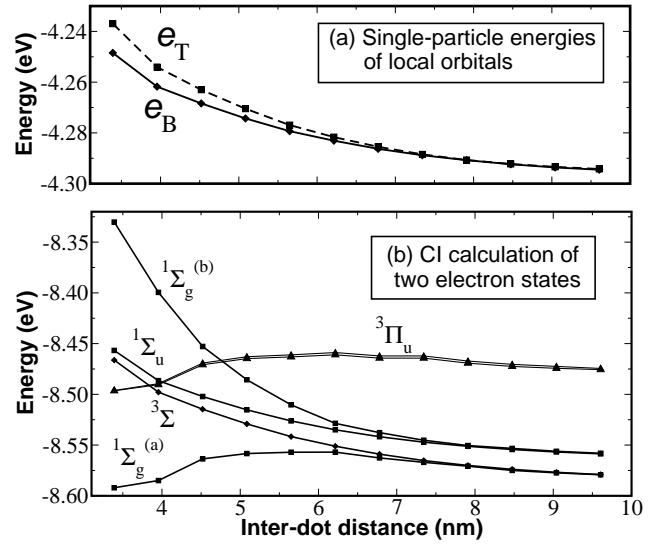


FIG. 2: (a) The effective single-particle energy levels e_T and e_B of dot-centered orbitals on the top dot and bottom dot respectively. (b) Energy of two-electron states calculated from CI using all constrained molecular orbitals.

gies, effective masses, hydrostatic and biaxial deformation potentials, and band-sets. The Schrödinger equation is solved by the Linear Combination of Bulk Bands (LCBB)²⁰ method in a basis of $\psi_{n,k}(\mathbf{r})$ of Bloch orbitals, i.e. $\psi_i(\mathbf{r}) = \sum_{n,k} C_{n,k}^{(i)} \psi_{n,k}(\mathbf{r})$ of band index n and wave vector k of material ($= \text{InAs, GaAs}$), strained uniformly to strain ϵ . We use $\epsilon = 0$ for the (unstrained) GaAs material, and an average ϵ value from VFF for the strained dot material (InAs). For the InAs/GaAs system, we use $n = 2$ for electron states on a $6 \times 6 \times 28$ k-mesh. Unlike the effective-mass description of single-particle state used for electrostatic dot,^{9,10,11,12} here we allow inter-band and inter-valley coupling.

Single-particle symmetry breaking: Figure 1b shows the single-particle dot-molecule energy levels as a function of inter-dot distance d . These results can be generally understood using bonding/antibonding molecular orbitals as shown in Fig. 1c. At large d , the energy levels converge to those of single dots, showing an s-level and, at $\delta_{\text{sp}} = 106$ meV higher, two p-levels split by a few meV reflecting the atomistic C_{2v} symmetry of the cylindrically symmetric dots²³. Bonding and antibonding molecular orbitals form when the two dots interact: the two single-dot s orbitals form molecular σ_g and σ_u orbitals, whereas the four single-dot p orbitals (two on each dot) form two molecular σ_u and two molecular σ_g orbitals.¹² Note that the splitting of σ_g from σ_u is not symmetric, as can be seen by looking at the average of both energies in Fig. 1b (dashed line). The average energy increases with decreasing interdot separation in response to the strain exerted by the presence of the other dot (Fig. 1a). Beyond this overall effect, the strain field

is different on both geometrically identical dots because the dots are non-spherical (Fig. 1a) and lack inversion symmetry. This causes a "symmetry breaking" of the molecular orbitals at short interdot distances. At $d = 3.4$ nm, we found that the bonding (antibonding) states are mostly localized on the bottom (top) dot. In previous effective-mass calculations,^{7,8,11,12,13} strain effects were not included and single-particle symmetry-breaking was not found.

A more quantitative analysis of the symmetry breaking can be given when the molecular orbitals are transformed via a Wannier-like transformation into single dot states. These can be obtained from a unitary rotation of molecular orbitals i ,

$$u_{1p} = \sum_i U_{1p}^{(i)} i; \quad (1)$$

where, i is the i -th molecular orbital and u_{1p} are the rotated, dot-centered orbitals (the l th orbital localized on $p = T$ or B dot). U are unitary matrices, $U^\dagger U = I$, chosen to maximize the total self-Coulomb energy.^{24,25} Once $U_{1p}^{(i)}$ are known, we define the orbital energies of the dot-centered states u_{1p} as:

$$e_{1p} = \hbar u_{1p} \hat{T} u_{1p} = \sum_i (U_{1p}^{(i)})^\dagger U_{1p}^{(i)} i; \quad (2)$$

where \hat{T} is the kinetic energy operator, and i is the energy of the i -th molecular orbital. The energies e_{1p} of the dot-centered orbitals are depicted in Fig. 2a as a function of the interdot separation. We see that the single-particle energies for both B and T orbitals rise quickly as the inter-dot distance is reduced, but the energy of the top dot orbital raises faster. At $d = 3.4$ nm, there is an energy splitting of 12 meV between top and bottom dot orbitals, which causes the asymmetry of the wave functions between top and bottom dots.

Many-particle symmetry-breaking: Having obtained the "molecular", single-particle energy (Fig. 1b), and wave functions, we calculate all interelectronic Coulomb and exchange integrals J and K of i by numerical integration²⁶, and set up a screened configuration-interaction expansion²⁷. A microscopic position-dependent dielectric screening²⁷ is applied to both Coulomb and exchange integrals to represent the inner electrons that are not calculated explicitly. Considering six molecular orbitals g, u, u, g of Fig. 1b, we have a total of 66 Slater determinants. The many-body wave functions are written as linear combinations of these determinants j_{ci} as, $= \sum_c A(c) j_{ci}$. The resulting many-particle energies are shown as a function of interdot separation in Fig. 2b. The energy splittings J_{ST} between the ground state singlet 1^1_g ^(a) and triplet 3^3 ranges from 1–100 meV and is much larger than in electrostatic dot molecules (< 1 meV).^{4,5,6} In Fig. 3a we decompose the two-electron wave functions into the leading configurations $1 = j_g^+ j_u^-, 2 = j_g^+ j_u^+, 3 = j_g^- j_u^+$, and $4 = j_u^- j_u^+$. The ground state is the singlet

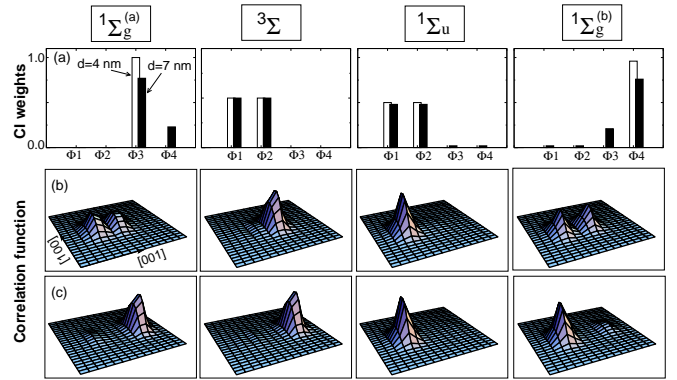


FIG. 3: (Color online) Panel (a) gives the weights of configurations $1, 2, 3$ and 4 of the many-particle CI wave functions. Panels (b) and (c) depict the probability of finding the second electron at position r given that the first electron has been found on the center of the bottom dot for the interdot distances (b) $d = 4$ nm and (c) $d = 7$ nm.

1^1_g ^(a) state, followed by the three-fold degenerated triplet states³ (we depict only the $s_z = 0$ state made of $1^1_g + 2^1_g$ in Fig. 3) and the next singlets 1^1_u (made of $1^1_g - 2^1_g$) and 1^1_g ^(b). To explore the localization of these states, we plot in Fig. 3b and 3c, the pair correlation functions $P(r_0; r) = j_{ci}^0(r_0; r)^2$ where r_0 is fixed at the center of the bottom dot. $P(r_0; r)$ gives the probability of finding the second electron at position r given that the first electron has been found at r_0 . For the ground state singlet 1^1_g ^(a), we see that at the small interdot separation $d = 4$ nm, the probability to find the second electron in the top or the bottom dot are comparable, suggesting a molecular-like delocalized state. Accordingly, the wave function analysis reveals a dominant contribution from the product of two delocalized molecular orbitals 3^3 . However with increasing interdot separation, the electrons show correlation induced (i.e. the coupling between 3^3 and 4^3) localization. At $d = 7$ nm, the second electron is almost entirely localized on the top dot as shown in Fig. 3c. A similar delocalized to localized transition applies for the 1^1_g ^(b) state, with the difference, that at large d both electrons are localized on the same (bottom) dot. In contrast, the triplet states 3^3 and the singlet 1^1_u show localization at all interdot distances. For the triplet states the two electrons are localized on different dots while for 1^1_u both electrons are localized on the same dot.

To understand the (hidden) broken-symmetry in the many-particle CI wave functions, and to study the degree of localization quantitatively, we resort to the Wannier-like transformation of Eq. (1). The CI matrix elements expressed initially in the molecular basis i [Eq. (1)] are transformed into the dot-centered Wannier basis 1_{1p} [Eq. (1)]. For example, $f j_{1p}^0; 1^0_{1p} j^0$ denotes the configuration where one electron is on the l th orbital of the p dot with spin $+$, and the other electron is on the l' th orbital of the p^0 dot with spin 0 . The two electrons can

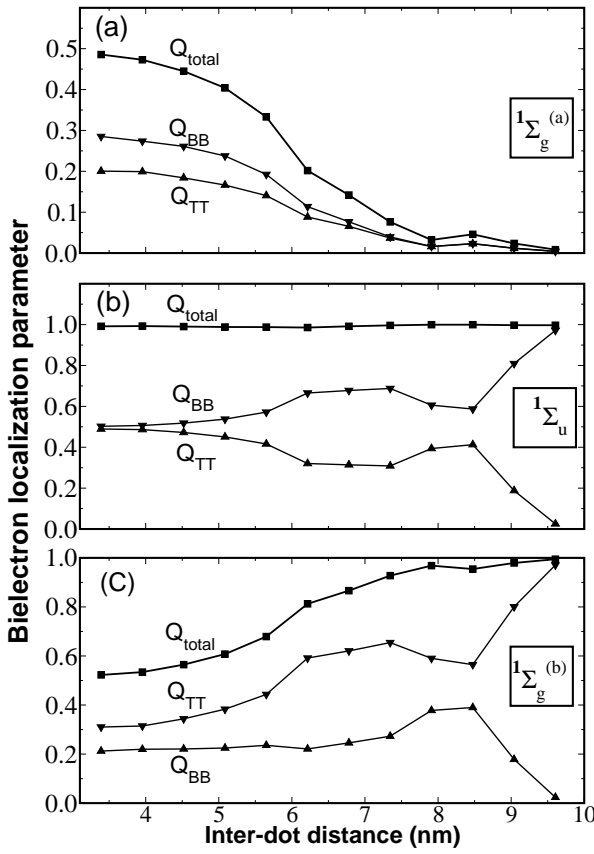


FIG. 4: The probability of two electrons occupying the same dot [Eq.(3)] for (a) $1\Sigma_g^{(a)}$, (b) $1\Sigma_u$, (c) $1\Sigma_g^{(b)}$ states. Q_{TT} (Q_{BB}) is the probability of both electrons being on the top (bottom) dot, while Q_{total} gives the total probability.

be either both on the top dots, or both on the bottom dots, or one on the top and the other on the bottom dots. We can thus define a "bielectron localization parameter" $Q_{pp}^{(i)}$ as the probability of two electrons occupying the dot p (T or B) at the same time in the many-particle state i ,

$$Q_{pp}^{(i)} = \sum_{j_1, j_2} P(j_1, j_2; i); \quad (3)$$

where $P(C)$ is the weight of the configuration C in the many-body wave functions of state i . The total probability of two electrons being on the same dot is then $Q_{total}^{(i)} = Q_{TT}^{(i)} + Q_{BB}^{(i)}$ for the i -th state. Figure 4, shows the bielectron localization parameter $Q_{pp}^{(i)}$ of Eq.(3) for the many-particle states $i = 1\Sigma_g^{(a)}, 1\Sigma_u, 1\Sigma_g^{(b)}$. We see that: (i) For the ground state $1\Sigma_g^{(a)}$ (Fig. 4a), $Q_{BB} > Q_{TT}$ at all inter-dot separations (as is the case for the $1\Sigma_u$ state), whereas

for state $1\Sigma_g^{(b)}$ (Fig. 4c), we always have $Q_{TT} > Q_{BB}$, indicating symmetry breaking for these many-body wave functions. (ii) The ground state $1\Sigma_g^{(a)}$ has a very small Q_{pp} at large inter-dot separation ($d > 8$ nm), whereas for $1\Sigma_g^{(b)}$, the probability of two electrons being on the same dot is close to 1. At smaller d , Q_{total} increases rapidly for $1\Sigma_g^{(a)}$, while it decreases for $1\Sigma_g^{(b)}$. (iii) The calculated $Q_{pp}^{(3)}$ are zero (not shown), and the two electrons are therefore always on different dots (suggesting that the coupling between 3 and higher triplet configurations is negligible). This is very different from the situation in large electrostatic quantum dot molecules^{4,5,6} (with $J_{ee} > J_{eJ}$) where the lowest 3 state is expected to mix with higher energy triplet configurations and acquire non-zero double electron occupations $Q_{pp}^{(3)} > 0$. (iv) $Q_{total}^{(1\Sigma_u)}$ is close to 1 for all inter-dot distances (Fig. 4b) and both electrons are therefore occupying the same dots.

As we have noted in the introduction, quantum computing based on two spins in dot molecules requires that (i) $Q_{total}^{(i)} < 1$ i.e. the electrons should be localized on different dots as much as possible. We now see this is satisfied for $1\Sigma_u$, but not for the singlets $1\Sigma_u$ and $1\Sigma_g^{(b)}$. For $1\Sigma_g^{(a)}$, we find $Q_{total}^{(i)} < 1$ only at large inter-dot separation d . (ii) Two spins should have high entanglement. Since entanglement is maximized for pure singlet and triplet states without double-occupancy (i.e. $Q_{pp} = 0$), this also requires that $Q_{pp}^{(i)} < 1$. (iii) The inter-dot separation should be such that significant singlet-triplet splitting should exist. Conditions (i) and (ii) require large inter-dot separation d , while (iii) requires small d . Considering all the present results, the requirements for quantum computation are best met for the ground state $1\Sigma_g^{(a)}$ at an inter-dot distance of 6 to 8 nm, where we have significant J_{eJ} , and Q_{total} is small.

To conclude, we investigated both single-particle and many-particle wave function symmetry-breaking in the quantum dot molecules made of two identical, vertically stacked InAs/GaAs self-assembled quantum dots. For single-particle states, we find a strained-induced symmetry breaking at short interdot separations. For many-particle states, we find that two electrons are always on different dots in the triplet state, while for the ground state singlet, the probability of "bielectron localization" is not zero and increases rapidly as the two dots come close to each other. The ideal interdot separation where the two electron spins can be used for quantum information is around 7 nm. At this distance the singlet-triplet splitting is large but the double electron occupation still low.

This work was supported by US DOE-SC-BES-DMR, grant no. DEAC 36-98-GO 10337.

¹ D. P. DiVincenzo, Science 270, 255 (1995).

² D. Loss and D. P. DiVincenzo, Phys. Rev. A 57, 120

(1998).

³ J. Schliemann, D. Loss, and A. H. MacDonald, *Phys. Rev. B* **63**, 085311 (2001).

⁴ R. C. Ashoori, H. L. Stormer, J. S. Werner, L. N. Pfeiffer, S. J. Pearton, K. W. Baldwin, and K. W. West, *Phys. Rev. Lett.* **68**, 3088 (1992).

⁵ A. T. Johnson, L. P. Kouwenhoven, W. de Jong, N. van der Vaart, and C. J. P. M. Harmans, *Phys. Rev. Lett.* **69**, 1592 (1992).

⁶ S. Tarucha, D. G. Austing, T. Honda, R. J. van der Hage, and L. P. Kouwenhoven, *Phys. Rev. Lett.* **77**, 3613 (1996).

⁷ M. Pi, A. Emperador, M. Barranco, F. G. Garcias, K. M. Muraki, S. Tarucha, and D. G. Austing, *Phys. Rev. Lett.* **87**, 066801 (2001).

⁸ M. Rontani, S. Amaha, K. Muraki, F. M. Anghie, E. M. Olinari, S. Tarucha, and D. G. Austing, *Phys. Rev. B* **69**, 085327 (2004).

⁹ L. R. C. Fonseca, J. L. Jimenez, J. P. Leburton, and R. M. Martin, *Phys. Rev. B* **57**, 4017 (1998).

¹⁰ S. Bednarek, B. Szafran, K. Lis, and J. Adamowski, *Phys. Rev. B* **68**, 155333 (2003).

¹¹ X. Hu and S. D. Sarma, *Phys. Rev. A* **61**, 62301 (2000).

¹² M. Rontani, F. Troiani, U. Hohenester, and E. M. Olinari, *Solid State Comm.* **119**, 309 (2001).

¹³ C. Yannouleas and U. Landman, *Phys. Rev. Lett.* **82**, 5325 (1999).

¹⁴ D. Bimberg, M. Gundmann, and N. N. Ledentsov, *Quantum Dot Heterostructures* (John Wiley & Sons, 1999).

¹⁵ T. Ota, M. Stopa, M. Rontani, T. Hatano, K. Yamada, S. Tarucha, H. Song, Y. Nakata, T. Miyazawa, T. Ohshima, et al., *Superlattices and Microstructures* **34**, 159 (2003).

¹⁶ T. Ota, K. Ono, M. Stopa, T. Hatano, S. Tarucha, H. Z. Song, Y. Nakata, T. Miyazawa, T. Ohshima, and N. Yokoyama, *Phys. Rev. Lett.* **93**, 66801 (2004).

¹⁷ P. N. Keating, *Phys. Rev.* **145**, 637 (1966).

¹⁸ J. L. Martins and A. Zunger, *Phys. Rev. B* **30**, 6217 (1984).

¹⁹ A. J. Williamson, L.-W. Wang, and A. Zunger, *Phys. Rev. B* **62**, 12963 (2000).

²⁰ L.-W. Wang and A. Zunger, *Phys. Rev. B* **59**, 15806 (1999).

²¹ H. Fu, L.-W. Wang, and A. Zunger, *Appl. Phys. Lett.* **71**, 3433 (1997).

²² L.-W. Wang, A. J. Williamson, A. Zunger, H. Jiang, and J. Singh, *Appl. Phys. Lett.* **76**, 339 (2000).

²³ G. Bester and A. Zunger, *Phys. Rev. B* (in press).

²⁴ C. Edmiston and K. Ruedenberg, *Rev. Mod. Phys.* **35**, 457 (1963).

²⁵ L. He, G. Bester, and A. Zunger, to be published.

²⁶ A. Franceschetti and A. Zunger, *Phys. Rev. Lett.* **78**, 915 (1997).

²⁷ A. Franceschetti, H. Fu, L.-W. Wang, and A. Zunger, *Phys. Rev. B* **60**, 1819 (1999).